Computers and Mathematics with Applications 57 (2009) 169–183

Contents lists available at ScienceDirect

Computers and Mathematics with Applications

journal homepage: www.elsevier.com/locate/camwa

Realization of an autonomous integrated suite of strapdown astro-inertial navigation systems using unscented particle filtering

Jamshaid Ali *, Fang Jiancheng [1]

School of Instrumentation Science and Optoelectronics Engineering, Beijing University of Aeronautics and Astronautics, Beijing - 100083, China

ARTICLE INFO

Article history:
Received 30 March 2006
Received in revised form 22 November 2007
Accepted 10 July 2008

Keywords:
Astro-inertial navigation
Multisensor data synthesis
Nonlinear system
EKF
UKF
UPF

ABSTRACT

Multisensor navigation data synthesis (MNDS) is the process of fusing outputs from inertial sensors with information from other sensors and information processing blocks into one representational form. This technique is anticipated to accomplish enhanced accuracy and more specific inferences than could be achieved by the use of a single sensor alone. Therefore, this research work expounds innovative filtering methodology for the multisensor navigation data synthesis for a ballistic missile application that augments navigation system performance. The premise and characteristics of strapdown inertial navigation system (SINS) integrated with the astronavigation system (ANS) based on the unscented particle filter (UPF) are investigated in this paper. Configuration of the integrated navigation system is presented with its canonical model, and system dynamic and stochastic models required for the filtering algorithm are presented. To exemplify integrated navigation filter mechanization is the foremost aspiration of this research. To validate and corroborate the designed MNDS technique, simulations are carried out that demonstrate the validity of this method on enhancing the navigation system's accuracy with estimation and compensation for the gyro's drift. This integrated system results in a significant reduction in impact-point dispersion of a re-entry vehicle.

1. Introduction

The guidance of a vehicle is accomplished by the most promising strapdown inertial navigation system (SINS). It has the advantage of fast in-flight response and it gives good data on short term changes in attitude, position and velocity. The distinguishing features of space missions are the long times of flight and the large expenditure of propulsion energy. Since these features affect the resultant gyro drift and accelerometer errors, it is usually necessary to periodically update the SINS data by external aiding information. It is convenient to employ systems which do not require external cooperation of active system elements of any kind; these are known as self-contained systems [1].

For space exploration missions and defense requirements, spacecraft and ballistic missiles are employed. A spacecraft is a precisely guided rocket-propelled vehicle. It is manned or unmanned and is designed to be placed into an orbit about the earth or into a trajectory to another celestial body. A ballistic missile is also a rocket-propelled vehicle flying in orbits outside the atmosphere of the earth but restrained to the earth by its gravitational field. With the help of guidance and control mechanisms, it can deliver an explosive warhead with a great accuracy [1]. The obvious vehicle-borne inertial references are the stars, which may be imaged by star sensors to periodically correct the gyro-controlled coordinate system. Therefore, the ANS as a self-contained aiding source, in current and prior sense, is based on astronomical observations made using charge

* Corresponding author. Tel.: +86 10 82330114.
E-mail addresses: jimmi4u@hotmail.com (J. Ali), fangjiancheng@buaa.edu.cn (J. Fang).
[1] Tel.: +86 10 82338058; fax: +86 10 82338058.

0898-1221/$ – see front matter © 2008 Elsevier Ltd. All rights reserved.
doi:10.1016/j.camwa.2008.07.042

coupled device (CCD) based electro-optical star sensors [2]. Also, this autonomous suite of ANS is free from radio aids, which may be unreliable, jammable, or unavailable during a wartime encounter. Consequently, SINS integrated with ANS using a nonlinear filtering technique is a subject matter of this paper.

Although, the global positioning system (GPS) has received much attention for providing augmentation for SINS, an autonomous sensor is always preferable because active sensors such as the GPS may be unavailable as a result of hostile attacks on, or reliability failure of radio based navigation aids during the critical phase of the mission. The fact that the C/A (coarse acquisition) code of a commercial GPS receiver is a simple length 1023 linear polynomial that is public knowledge makes it possible to jam the system. Moreover, the current missile technology control regime (MTCR) export control limits the sale of GPS receivers that can function at speeds in excess of 515 m/s (1000 nm/h) and altitudes greater than 18 km (60,000 ft). As a result, for third world countries, it is impracticable to purchase and use these controlled GPS receivers for its defense program. Therefore, in this study, we suggest error compensation scheme for SINS using attitude information estimated by the ANS computer.

The extended Kalman filter (EKF) has been used as the standard navigation data synthesis technique. It is applied to nonlinear filtering problems. As a result, its performance relies on, and is limited by the linearizations performed on the concerned model. The equations for the SINS errors are nonlinear and the ANS measurements are also nonlinear. Generally, the EKF for integrated navigation system has fairly good estimation performance. When errors in the ANS measurements and in inertial sensors are not Gaussian, the EKF based SINS/ANS integration suffers from performance degradation. The EKF makes a Gaussian assumption on the probability density of the state random variable. Often this assumption is valid, and numerous real-world applications have been successfully implemented based on this assumption [3].

The particle filtering (PF), known as a nonlinear filtering method, may cope with nonlinear and non-Gaussian models. Its concept was originally proposed back in 1954 [4] in the form of the sequential Monte Carlo (SMC) estimation based on particle representation of probability densities. Since computational power has been tremendously increased during the past decades, the computational effort constraint in using PF has been eliminated. Recently, PF finds its applications in various fields such as wireless communication, target tracking, and navigation systems. The PF represents the stochastic nature of the system with a sampling of the probability distribution, which generates many particles, each representing one point in the probability space. The weight of each particle, which is updated and corrected whenever new measurements become available, represents the likelihood that this particle corresponds to the true system state. The deterministic dynamics are applied to each particle to predict the distribution at a future step.

One practical problem of particle filtering is the selection of the importance proposal distribution. In unscented particle filtering (UPF), the unscented Kalman filter (UKF) is used for the importance proposal generation. van der Merwe et al. have recently developed the unscented particle filter (UPF) in the field of filtering theory [5]. Based on this new development, in this paper, we introduce a direct approach to generate better proposal distributions for the proposed integrated navigation. The UPF is a parametric/non-parametric hybrid of UKF and particle filters. The particle filter part of the UPF provides the general probabilistic framework to handle nonlinear non-Gaussian systems, and the UKF part of the UPF generates better proposal distributions by taking into account the most recent observation. It is claimed by its developers that the UPF can outperform standard particle filters, EKF and UKF. The UPF may cope with nonlinear models without any limitation, and non-Gaussian noise as well.

In this paper, this new approach to optimal nonlinear filtering is presented, which is applied to the problem of SINS augmentation by ANS. This paper comprises 5 sections; integrated navigation system is the subject of Section 2; the UPF algorithm is presented with an overview of the particle filtering in Section 3; in Section 4, simulation and results of the proposed integration are presented; and some useful conclusions are drawn in Section 5.

2. The integrated navigation system configuration

A modern SINS generally comprises inertial sensors such as gyros and accelerometers which are fixed in a unit known as a strapdown inertial measurement unit (SIMU). The gyros measure angular rotation and allow the control of an analytical platform that has to remain fixed in a frame of reference. The accelerometers measure accelerations, which are projected onto this analytical platform and then integrated a first time, to give velocity, then a second time to give the position. The attitude is obtained by extracting the three angles that convert from the frame of reference of the vehicle to the frame of reference of the analytical platform. The precision of SINS depends directly on the errors of the inertial sensors and more specifically on the projection of these errors into the navigation frame of reference. The precision of SINS is therefore limited by the intrinsic precision of these sensors. In the case of long-term inertial navigation, the position errors depend in particular on the precision of the gyros.

Another very common attitude sensor type used in missions with very high attitude accuracy requirements is state of the art star sensors. These are electro-optical sensors and consist of CCD (charge coupled device) array detectors to search for and track up to six stars in an instrument dependent field of view (FOV). It allows images of several objects to be obtained in a single exposure with a specific integration time by transferring the photo charges of each pixel to an output stage. The charges are measured, digitized and read into the processor's memory one pixel at a time, row by row. After that the star identification and attitude determination can follow [6].

In a focused image on a CCD array, a star appears as a point source, because all luminous power from the star will end up in one pixel. By defocusing the image, stars will cover several pixels, depending on the brightness or magnitude of the star.

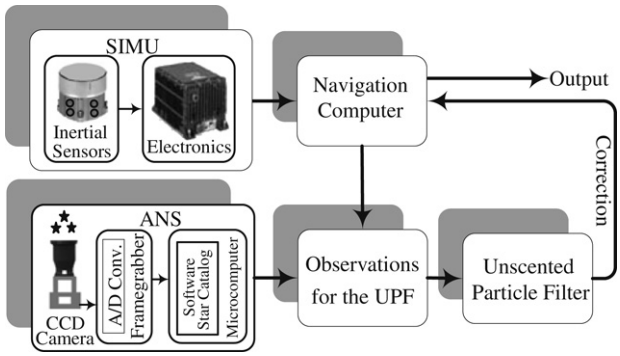

Fig. 1. Configuration for SINS/ANS data synthesis.

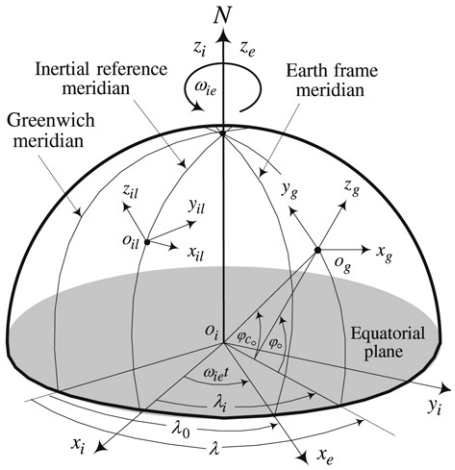

Fig. 2. Coordinate frames.

The summation of transferred charges of those pixels is proportional to the brightness of the star and with this information, the instrumental magnitude of the star is computed. These magnitudes and the star pattern on the chip are compared with a star catalog, which is aboard the navigating vehicle. The attitude determination is mostly done onboard the spacecraft with the mentioned star catalog by a powerful microprocessor. The functional flow for a star sensor unit integrated with SINS is shown in Fig. 1. The attitude determination process is simply a vector based approach by connecting the measured stars in the body reference frame to known star directions in the inertial reference frame [6].

It is easy to see that this sensor combination is an ideal way to improve the specific disadvantages of each sensor type and to show that the combination and data fusion is more powerful than just the adding of both sensors aboard a spacecraft. For a long-duration space flight, the SINS/ANS combination provides a nearly all-weather, un-jammable and precise navigation system. The inertial system would slowly drift-off; the astro system will stabilize it against that drift, but the astro system must require the short-term stability of the inertial system to stabilize its reference frame.

2.1. Coordinate frames

Definitions of the frames employed in this paper are given below [1,2,7,8]. Fig. 2 depicts relationship between the different frames.

(1) The earth-centered earth fixed frame (e-frame) is used for defining the position. It has its origin at the center of the earth. The x-axis points to the point of intersection of mean Greenwich meridian and equatorial plane; the z-axis is perpendicular to mean equatorial plane pointing towards the North Pole; and the y-axis completes a right-handed system.

(2) The geocentric inertial frame (i-frame) has its origin at the center of the earth and is non-rotating with respect to the fixed stars. Its x-axis is in the equatorial plane and the z-axis is normal to that plane; and the y-axis completes a right-handed system. In this paper, the x-axes of the e- and the i-frame are so arranged that they are coincident at the navigation starting time, $t = 0$. After the launch of the vehicle, for time $t > 0$, the angle (α) between them varies in accordance with $\alpha = \omega_{ie}t$, where ω_{ie} is the earth's rate.

(3) The launch-inertial frame (*il*-frame) has its origin at the launch point. Its *z*-axis is vertical upward and normal to the reference ellipsoid; the *y*-axis is horizontal and lies in nominal launch plane; and the *x*-axis is horizontal and perpendicular to nominal launch plane, rightward.
(4) The body frame (*b*-frame) has its origin at the center of mass of the vehicle. Its *x*-axis points along longitudinal axis of the vehicle; the *z*-axis is perpendicular to the longitudinal plane of symmetry; and the *y*-axis completes a right-handed system.
(5) Local level or geographic frame (*g*-frame) has its origin at the location of navigation system of vehicle and its axes are aligned with the east, north and upward directions. Upward is defined to be normal to the reference ellipsoid.

In Fig. 2, λ = terrestrial longitude from Greenwich; λ_0 = initial terrestrial longitude; λ_i = celestial longitude; φ_0 = initial geographic latitude; and φ_{c_0} = initial geocentric latitude.

2.2. Inertial navigation system errors

Two major sources of error in the missile's inertial navigation system are [9]:

2.2.1. Gyros drift

Drift of the missile's gyros results in a rotation of the missile's reference coordinate frame, and consequently alignment error with respect to the reference navigation coordinate frame. The drift angles about axes located along the reference navigation frame are given by the equation

$$\delta\theta^{il}_{g,i} = \int_0^{t_f} \delta\dot{\theta}^{il}_{g,i}\mathrm{d}t, \quad i = x, y, z \tag{1}$$

where g stands for gyro; and t_f is the time of flight with launch-time as zero reference.

The drift rate $\delta\dot{\theta}_g$ in the above equation has both constant and acceleration-sensitive components. Drift of the missile gyros also causes position error, which is given in the reference navigation frame as

$$\begin{aligned}
\delta r^{il}_{x_g} &= \int_0^{t_f}\int_0^{t_f} a^{il}_y \delta\theta^{il}_{g_z}\mathrm{d}t\mathrm{d}t + \int_0^{t_f}\int_0^{t_f} a^{il}_z \delta\theta^{il}_{g_y}\mathrm{d}t\mathrm{d}t \\
\delta r^{il}_{y_g} &= \int_0^{t_f}\int_0^{t_f} a^{il}_x \delta\theta^{il}_{g_z}\mathrm{d}t\mathrm{d}t + \int_0^{t_f}\int_0^{t_f} a^{il}_z \delta\theta^{il}_{g_x}\mathrm{d}t\mathrm{d}t \\
\delta r^{il}_{z_g} &= \int_0^{t_f}\int_0^{t_f} a^{il}_y \delta\theta^{il}_{g_x}\mathrm{d}t\mathrm{d}t + \int_0^{t_f}\int_0^{t_f} a^{il}_x \delta\theta^{il}_{g_y}\mathrm{d}t\mathrm{d}t
\end{aligned} \tag{2}$$

where a_x, a_y, a_z are the components of missile acceleration parallel with the axes of the reference navigation frame.

2.2.2. Inaccuracies in accelerometers

The position error caused by the inaccuracies of the missile accelerometers is expressed with respect to the navigation frame as [9].

$$\delta r^{il}_{a,i} = \int_0^{t_f}\int_0^{t_f} (\delta a^{il})_i \mathrm{d}t\mathrm{d}t, \quad i = x, y, z \tag{3}$$

where a stands for the accelerometer and δa is the error in indication of missile's acceleration along the three coordinate directions.

2.3. SINS nonlinear error model

The purpose of the inertial navigation systems (INS) is to provide the position, velocity and attitude of the vehicle through self-contained sensors in a convenient coordinate system. The position, velocity and attitude information in an INS, however, is not exact due to many error sources such as sensor inaccuracies, initial alignment errors, sensor mount misalignments and computational errors. The error growth rate is one of the most important factors that affects the performance of an INS. For this reason, a considerable amount of the work has been performed in the field of INS which concentrates on the error analysis. The basis of the error analysis is, of course, the error model that describes the propagation of the errors. The model, besides being the tool for the error analysis, also plays an important role in the implementation of integration filters and in the real time failure detection [10].

The conventional linearized error models of SINS are found not to be effective to represent the nonlinear characteristics of navigation error propagation in case of a system which causes large navigation errors. To represent a large attitude error of the SINS, the axes misalignment angles are introduced and the relationships the velocity, position and attitude errors are derived [11,12].

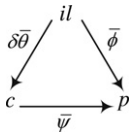

Fig. 3. Error analysis schema.

In this paper, space-stabilized mechanization is used for the SINS implementation and its error model. This mechanization has been used for years in missiles [13]. It is conceptually the simplest of all possible system implementations, since Newton's laws are most simply stated in an inertial frame of reference. The space-stabilized inertial navigation system outputs navigation parameters in an inertially non-rotating frame. Thus, this mechanization is free of the earth's rotation and transport rate [7]. This section will give error analysis of the space-stabilized SINS which will consider the effect of all of the known major error sources: i.e. gyro drift, accelerometer bias, and gravity anomalies.

2.3.1. Attitude error model

A measure of the quality of any INS is some weighted combination of its attitude, position and velocity indication capabilities, depending upon the mission involved. The gyros measure the vector of inertial rotation and the system uses it to calculate attitude in the form of a coordinate transformation matrix. Inevitably, accelerometer and gyro errors occur in the measured vectors. As a result of gyro measurement error, an error in the transformation matrix occurs [14].

The error analysis schema, shown in Fig. 3, portrays the relationship between different frames. Here, c and p refer to the computed and analytical platform frame, respectively. It is obvious that 'c' follows 'il', 'p' follows 'c' and 'p' follows 'il' indirectly. There is misalignment between the 'il' and 'p' frames that is expressed by rotation angles ϕ_x, ϕ_y, ϕ_z. Therefore, the estimated attitude matrix C_b^p from the SINS is expressed as

$$\hat{C}_b^{il} = C_{il}^p C_b^{il} = C_b^p. \tag{4}$$

The attitude error in space-stabilized SINS mechanization is the orthogonal transformation error between the b- and il-frame. In this perspective, attitude error equation can be articulated as a nonlinear attitude error model of SINS. For large attitude errors, the relationship between p- and il-frame is obtained by three successive rotations of il-frame by angles ϕ_x, ϕ_y, ϕ_z about x, y and z axes respectively as

$$C_{il}^p = \begin{bmatrix} c_y c_z & c_y s_z & -s_y \\ s_x s_y c_z - c_x s_z & s_x s_y s_z + c_x c_z & s_x c_y \\ c_x s_y c_z + s_x s_z & c_x s_y s_z - s_x c_z & c_x c_y \end{bmatrix} \tag{5}$$

where $c_x = \cos\phi_x$, $c_y = \cos\phi_y$, $c_z = \cos\phi_z$, $s_x = \sin\phi_x$, $s_y = \sin\phi_y$, and $s_z = \sin\phi_z$.

Angular velocity of the mathematical p-frame relative to the i-frame is equal to the angular velocity of the il-frame relative to the i-frame plus angular velocity of the p-frame relative to the il-frame and all coordinated in the p-frame. This relationship is described as

$$\bar{\omega}_{ip}^p = \bar{\omega}_{iil}^p + \bar{\omega}_{ilp}^p. \tag{6}$$

Here, $\bar{\omega}_{ilp}^p$ represents the angular rate of the il-frame through axes misalignment angles: i.e. $\bar{\omega}_{ilp}^p = \dot{\bar{\phi}}^{il}$, and $\bar{\omega}_{iil}^p = C_{il}^p \bar{\omega}_{iil}^{il}$ where $\bar{\omega}_{iil}^{il} = 0$ as the i- and il-frames are inertially fixed. Therefore Eq. (6) becomes

$$\bar{\omega}_{ip}^p = \dot{\bar{\phi}}^{il} \quad \text{or} \quad \dot{\bar{\phi}}^{il} = \bar{\omega}_{ip}^p. \tag{7}$$

In the above relationship, $\bar{\omega}_{ip}^p = C_b^p \bar{\varepsilon}^b$, defining $\bar{\varepsilon}^b = \bar{\varepsilon}_c^b + \bar{\varepsilon}_r^b$, where $\bar{\varepsilon}_c^b$ and $\bar{\varepsilon}_r^b$ representing the constant and random drift, respectively.

$$\text{Thus, } \hat{\dot{\bar{\phi}}}^{il} = \hat{C}_b^{\,il}(\bar{\varepsilon}_c^b + \bar{\varepsilon}_r^b). \tag{8}$$

$$\text{Hence, } \hat{\dot{\bar{\phi}}}^{il} = \dot{\bar{\phi}}^{p} = \hat{C}_b^{\,il}(\bar{\varepsilon}_c^b + \bar{\varepsilon}_r^b) = C_{il}^p C_b^{\,il}(\bar{\varepsilon}_c^b + \bar{\varepsilon}_r^b). \tag{9}$$

2.3.2. Velocity error model

The basic measurement equation of the system is for the specific force measured by the accelerometers, namely

$$\dot{\bar{v}}^{il} = C_b^{il}\bar{f}^b + \bar{g}^{il} \tag{10}$$

where $\bar{f}$ is the specific force measured by accelerometers; $\bar{g}$ is the mass attraction gravity; and C_i^{il} is a constant transformation matrix between the indicated frames and is estimated through $C_i^{il} = C_{g_0}^{il} C_i^{g_0}$. Here, g_0 stands for the g-frame at the start of navigation process.

Perturbation of the acceleration equation yields

$$\delta\dot{\bar{v}}^{il} = \delta C_b^{il}\bar{f}^b + C_b^{il}\delta\bar{f}^b + C_i^{il}\delta\bar{g}^i. \tag{11}$$

The symbol δ is used to denote perturbations. The above equation indicates that the error in the transformed acceleration equals the error in measuring the specific force and resolving it into the true navigation frame plus the error in gravity computation. The term $\delta\bar{f}^b$ is accelerometer measurement error composed of a constant and a random bias. The term $\delta\bar{g}^i$ is due to inaccurate knowledge of the earth's gravitational field and inaccuracies in the vehicle's position [13]. In the velocity error model, the quantity $\delta C_b^{il}\bar{f}^b$ is strongly related to the attitude error. It is important to compute this term to describe the correlated relationship between the attitude error and the velocity error [12].

Perturbed attitude transformation matrix is defined by

$$\hat{C}_b{}^{il} = C_b^{il} + \delta C_b^{il}. \tag{12}$$

Here, we are concerned about δC_b^{il}, which is the difference between the estimated transformation matrix and true attitude matrix. This attitude perturbation matrix, in terms of attitude error angles, is given as

$$\delta C_b^{il} = \hat{C}_b{}^{il} - C_b^{il} = C_{il}^p C_b^{il} - C_b^{il} = (C_{il}^p - I)C_b^{il}. \tag{13}$$

Thus, the velocity error model derived based on large navigation errors is

$$\delta\dot{\bar{v}}^{il} = (C_{il}^p - I)C_b^{il}\bar{f}^b + C_b^{il}(\bar{\nabla}_c^b + \bar{\nabla}_r^b) + C_i^{il}\delta\bar{g}^i \tag{14}$$

where $\bar{\nabla}_c^b$ and $\bar{\nabla}_r^b$ represent accelerometers' constant and random bias vectors, respectively.

In the simulation of SINS, a more accurate expression for the gravitational acceleration is employed with an ellipsoidal (or more precisely, spheroidal) earth model. Such a more precise approximation accounts for the earth's oblateness by including the second order gravitational harmonic term of the earth's gravitational field model. Perturbation variable $\delta\bar{g}^i$ is included in the error model and evaluation of its partial derivatives follows here:

$$\delta\bar{g}^i = \frac{\partial\bar{g}^i}{\partial\bar{r}^i}\delta\bar{r}^i = \begin{bmatrix} \partial g_x^i/\partial r_x^i & \partial g_x^i/\partial r_y^i & \partial g_x^i/\partial r_z^i \\ \partial g_y^i/\partial r_x^i & \partial g_y^i/\partial r_y^i & \partial g_y^i/\partial r_z^i \\ \partial g_z^i/\partial r_x^i & \partial g_z^i/\partial r_y^i & \partial g_z^i/\partial r_z^i \end{bmatrix} \begin{bmatrix} \delta r_x^i \\ \delta r_y^i \\ \delta r_z^i \end{bmatrix} = \begin{bmatrix} g_{11} & g_{12} & g_{13} \\ g_{21} & g_{22} & g_{23} \\ g_{31} & g_{32} & g_{33} \end{bmatrix} \begin{bmatrix} \delta r_x^i \\ \delta r_y^i \\ \delta r_z^i \end{bmatrix} \tag{15}$$

where:

$$\bar{g}^i = \begin{bmatrix} g_x \\ g_y \\ g_z \end{bmatrix} = -\frac{\mu}{r^3} \begin{bmatrix} \left\{1 + \frac{3}{2}J_2(r_e/r)^2[1 - 5(r_z^i/r)^2]\right\} r_x^i \\ \left\{1 + \frac{3}{2}J_2(r_e/r)^2[1 - 5(r_z^i/r)^2]\right\} r_y^i \\ \left\{1 + \frac{3}{2}J_2(r_e/r)^2[3 - 5(r_z^i/r)^2]\right\} r_z^i \end{bmatrix}. \tag{16}$$

In above equation, $r = \sqrt{(r_x^i)^2 + (r_y^i)^2 + (r_z^i)^2}$ is the magnitude of the geocentric position vector; r_x^i, r_y^i, r_z^i are the components of geocentric position vector; μ is the product of the earth's mass and universal gravitational constant and equals $(3.9860305 \pm 3 \times 10^{-7}) \times 10^{14}$ [m^3/s^2]; J_2 is a second-order harmonic constant coefficient of which the value is $(1.08230 \pm 0.0002) \times 10^{-3}$; and r_e is the earth's equatorial radius that equals 6378 137 [m]. The quantities μ, J_2 and r_e mentioned above are specific to the reference inertial frame for the SINS space-stabilized mechanization.

The indicated partial derivatives of gravitation with respect to the inertial position should include J_2 term if a more accurate form of the position error growth associated with the earth oblateness is desired. The partial derivative elements of gravitation with respect to position are defined as [15]

$$g_{11} = -\frac{g_x}{r} + 3(r_x^i/r)^2\left[\frac{g_x}{r} + \frac{\mu}{r^3}J_2(r_e/r)^2\left\{2\left(1 - 5(r_z^i/r)^2\right) - 1\right\}\right];$$

$$g_{12} = 3\frac{r_x^i r_y^i}{r^2}\left[\frac{g_x}{r} + \frac{\mu}{r^3}J_2(r_e/r)^2\left\{2\left(1 - 5(r_z^i/r)^2\right) - 1\right\}\right]$$

$$g_{13} = 3\frac{r_x^i r_z^i}{r^2}\left[\frac{g_x}{r} + \frac{\mu}{r^3}J_2(r_e/r)^2\left\{2\left(1-5(r_z^i/r)^2\right)+4\right\}\right];$$
$$g_{22} = -\frac{g_y}{r} + 3(r_y^i/r)^2\left[\frac{g_y}{r} + \frac{\mu}{r^3}J_2(r_e/r)^2\left\{2\left(1-5(r_z^i/r)^2\right)-1\right\}\right]$$
$$g_{23} = 3\frac{r_y^i r_z^i}{r^2}\left[\frac{g_y}{r} + \frac{\mu}{r^3}J_2(r_e/r)^2\left\{2\left(1-5(r_z^i/r)^2\right)+4\right\}\right]; \quad g_{21} = g_{12}; \quad g_{31} = g_{13}; \quad g_{32} = g_{23}; \quad \text{and}$$
$$g_{33} = -g_{11} - g_{22}.$$

2.3.3. Position error model

The position error equation for SINS in space-stabilized mechanization expressed in rectangular coordinates is given as [11]

$$\delta\dot{\bar{r}}^{il} = \delta\bar{v}^{il}. \tag{17}$$

2.4. Measurements using SINS/ANS attitude

An autonomous star sensor unit is used on spacecraft because it is capable of determining the attitude of the vehicle without having a priori attitude knowledge, and improved frequency of autonomous attitude updating. These capabilities are needed for future advanced attitude control and navigation systems along with improvements in reliability, mass, power, and cost. With technological advancements, it is possible to develop accurate star sensors with anti-blooming capable CCD, fast microprocessors, high density memory size, and efficient star identification algorithms. The functional flow for a star sensor has been shown in Fig. 1. The attitude determination process is simply a vector based approach by connecting the measured stars in the body reference frame to known star directions in the inertial reference frame [6]. This attitude information in conjunction with the attitude estimated by SINS serves as the measurement to the integration filter.

For a ballistic missile application, pre-launch attitude is maintained during the powered-phase. Prior to the final cut-off, when the vehicle gains altitude above earth's atmosphere, a star sensor images the stars. The observed attitude error is used to compute impact-point error both down-range and cross-range. Appropriate corrections are made for velocity errors which occur due to gyro's drift.

Attitude information from the space stabilized SINS is the transformation matrix C_b^{il} that is transformed to the *i*-frame. It is inevitable that the inertial sensing signals will be contaminated with uncertainties in a practical system. Consequently, only the computed transformation matrix $\hat{C}_b^{il}$ is available that differs from true matrix C_b^{il} due to axes misalignment angles as expressed by the following relationship [16]

$$\hat{C}_b^{il} = C_{il}^p C_i^{il} C_b^i. \tag{18}$$

Here, C_b^i is considered to be estimated from the ANS processing within the accuracy of the measurement process. Solving Eq. (18), the desired axes misalignment angles are estimated by

$$C_{il}^p = \hat{C}_b^{il}(C_i^{il}C_b^i)^{\mathrm{T}}\left[(C_i^{il}C_b^i)(C_i^{il}C_b^i)^{\mathrm{T}}\right]^{-1}. \tag{19}$$

3. The unscented particle filtering (UPF)

3.1. An overview of the particle filter

The use of Monte Carlo methods in filters can be traced back to 1969–70 [17,18]. The particle filter, known as a nonlinear filtering method, may cope with nonlinear and non-Gaussian models. It is an algorithm that provides iterative Monte Carlo approximations for a given sequence of state variable distribution. It approximates the required probability density function (pdf) by swarms of points in the state–space. These points are called particles. Each of the particles has an assigned weight and the state variable's distribution, can be approximated by a discrete distribution that depends on each of the particles. The probability assigned to each particle is proportional to the weight. These particles are random samples from the required pdf; so, with the number of particles increasing, they effectively provide a good approximation to the required pdf. Originally proposed by G. Salut, this method was first designed with birth and death of particles then with a constant number of particles, appeared for the first time in 1989 [19]. Since then, it has been extensively studied and applied [3,5,20,21].

A particle filter is a Markov chain Monte Carlo algorithm that approximates the system's state using a set of samples (particles), and keeps the distribution updated as new observations are made over time. To update the belief distribution given a new observation, the algorithm operates in three steps as follows [3–5]:

The sampling step: This step considers the evolution of the system over time. It uses a stochastic model of the system to generate a possible future state for each sample. This is performed by sampling a discrete mode, and then the continuous state given the new mode.

The re-weighting step: This corresponds to conditioning of the observations. Each sample is weighted by the likelihood of seeing the observations in the (updated) state represented by the sample. This step leads samples that predict the observations well to have high weight, and samples that are unlikely to generate the observations to have low weight.

The re-sampling step: To produce a uniformly weighted posterior, we then resample a set of uniformly weighted samples from the distribution represented by the weighted samples. In this re-sampling, the probability that a new sample is a copy of a particular sample is proportional to its weight, so high weight samples may be replaced by several samples, and low-weight samples may disappear.

3.2. Dynamic state–space model

The general state–space model can be divided into a state transition and state measurement model as [5]

$$x_{k+1} = f(x_k) + w_k \tag{20}$$

$$z_k = h(x_k) + v_k \tag{21}$$

where $x_k \in \mathbb{R}^{n_x} = [\bar{\phi}, \bar{v}, \bar{r}, \bar{\varepsilon}_c, \bar{\nabla}_c]^{\mathrm{T}}$ denotes the states of the system at temporal index k; $z_k \in \mathbb{R}^{n_z}$ represents observations those are axes misalignment angles; $w_k \in \mathbb{R}^{n_w}$ represent process noise; and $v_k \in \mathbb{R}^{n_v}$ is the measurement noise. The noises are assumed to be independent with their respective pdf, $p(w_k) = (x_k|x_{k-1})$ and $p(v_k) = (z_k|x_k)$ respectively. The states follow a first order Markov process and the observations are assumed to be independent given the states from the state process noise. The model under consideration is nonlinear and uses non-Gaussian regression. The prior distribution at $k = 0$, is denoted by $p(x_0)$. The posterior density $p(x_{0:k}|z_{1:k})$ constitutes the complete solution to the sequential estimation problem.

3.3. Unscented Kalman filtering

The unscented Kalman filter is a nonlinear, distribution approximation method. Its algorithm uses a finite number of sigma points to propagate the probability of state distribution through the nonlinear dynamics of system. The unscented transformation is a method for calculating the statistics of a random variable which undergoes a nonlinear transformation and builds on a principle that it is easier to approximate a probability distribution than an arbitrary nonlinear function. The UKF algorithm implemented with particle filter is given as [3,5]

1. Find weights for the states and covariance matrices as

$$\left.\begin{array}{l} W_0^s = \lambda/(n_s + \lambda) \\ W_0^c = (1 - \alpha^2 + \beta) + 0.5\lambda/(n_s + \lambda) \\ W_i^s = W_i^c = 0.5\lambda/(n_s + \lambda), \quad i = 1, \ldots, 2n_s \end{array}\right\} \tag{22}$$

where n_s is the number of the states in the augmented state vector; β is used to incorporate knowledge of the distribution of states, optimal value for Gaussian distribution is 2; s and c in the subscript and superscript denote state and covariance, respectively; and $\lambda = \alpha^2(n_s + \kappa) - n_s$ is a scaling parameter with α determining how the sigma points are spread, typical value is 10^{-3}, κ is a scaling parameter which can be used to incorporate up to fourth order precision in the transformation, usually set to zero.

2. Create a set of sigma points $\chi_{i,k-1}$ with $\hat{x}_{k-1}$ and P_{k-1}, using following set of equations

$$\left.\begin{array}{l} \chi_{0,k-1} = \hat{x}_{k-1}, \\ \chi_{i,k-1} = \hat{x}_{k-1} + (\sqrt{(n_s + \lambda)P_{k-1}})_i, \quad i = 1, \ldots, n_s \\ \chi_{i,k-1} = \hat{x}_{k-1} - (\sqrt{(n_s + \lambda)P_{k-1}})_i, \quad i = n_s + 1, \ldots, 2n_s \end{array}\right\} \tag{23}$$

where χ is the sigma points of the augmented state vector; and P_{k-1} is the old prediction of the covariance.

3. Prediction: the sigma points are then propagated through the nonlinear system and measurement models as

$$\chi_{k,k-1} = f(\chi_{k-1}) \tag{24}$$

$$\mathrm{Z}_{k,k-1} = h(\chi_{k-1}). \tag{25}$$

The prediction of the state and measurement vector as well as covariance of the state vector is performed as

$$\hat{x}_k^- = \sum_{i=0}^{2n_s} W_i^s \chi_{i,k|k-1}, \qquad \hat{z}_k = \sum_{i=0}^{2n_s} W_i^m \mathrm{Z}_{i,k|k-1} \tag{26}$$

$$P_k^- = \sum_{i=0}^{2n_s} W_i^c (\chi_{i,k|k-1} - \hat{x}_k^-)(\chi_{i,k|k-1} - \hat{x}_k^-)^{\mathrm{T}} + Q. \tag{27}$$

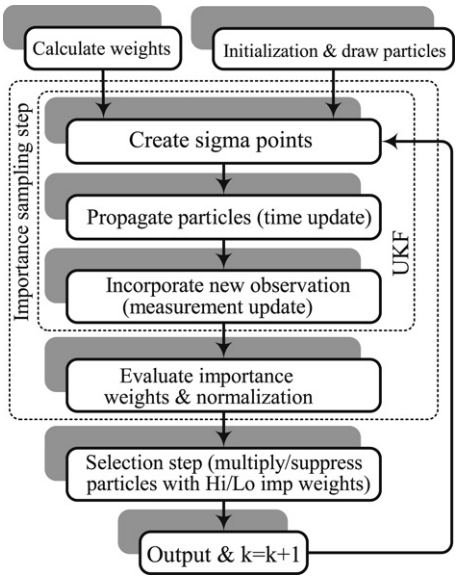

Fig. 4. The UPF algorithm.

4. Update: update the measurement prediction covariance, the cross covariance between the state and measurement, the Kalman gain, the state estimate, and the state covariance as

$$P_{\hat{z}_k\hat{z}_k} = \sum_{i=0}^{2n_s} W_i^c (\mathrm{Z}_{i,k|k-1} - \hat{z}_k)(\mathrm{Z}_{i,k|k-1} - \hat{z}_k)^{\mathrm{T}} + R \tag{28}$$

$$P^-_{\hat{x}_k^-\hat{z}_k} = \sum_{i=0}^{2n_s} W_i^c (\chi_{i,k|k-1} - \hat{x}_k^-)(\mathrm{Z}_{i,k|k-1} - \hat{z}_k)^{\mathrm{T}} \tag{29}$$

$$K_k = P_{\hat{x}_k^-\hat{z}_k} P^{-1}_{\hat{z}_k\hat{z}_k} \tag{30}$$

$$\hat{x}_k^+ = \hat{x}_k^- + K_k(z_k - \hat{z}_k) \tag{31}$$

$$\hat{P}_k^+ = P_k^- - K_k P_{\hat{z}_k\hat{z}_k} K_k^{\mathrm{T}}. \tag{32}$$

3.4. Unscented particle filtering algorithm

The UKF propagates the mean and covariance of the state distribution more accurately than the EKF and tends to generate better estimates of the true covariance of the state [5]. Furthermore, the distributions generated by the UKF generally have a broader overlap with the true posterior distribution compared with the EKF estimates which is partly due to the fact that the UKF computes the posterior covariance accurately to the third order (Gaussian prior) whereas the EKF uses a first order biased approximation. Furthermore, the UKF is able to scale the approximation errors in higher order moments of the posterior distribution allowing heavier tailed distributions. As the sigma points in the UKF are deterministically designed to capture certain characteristics of the prior distribution, it is possible to explicitly tune the algorithm to work on distributions that have heavier tails than Gaussian distributions. All in all, the UKF is more likely to generate more accurate proposal distributions within the particle filtering framework. Using the UKF as proposal distribution generator leads to the unscented particle filter (UPF) [5] (Fig. 4).

Implementation of the UPF, when the state process $\{x_k : k = 0, 1, 2, \ldots\}$ is described by a first-order Markov process, has a similar structure to the UKF. However, one major difference is that the unscented transformation (UT) is performed on a smaller dimensional random vector, since the state variable x_{t-1} is assumed fixed during each implementation of the transformation. Let $A_k = [\delta_k^{\mathrm{T}} \varepsilon_k^{\mathrm{T}}]^{\mathrm{T}}$, where δ_t and ε_t are independent with means, $E[\delta_k] = d_k$ and, $E[\varepsilon_k] = e_k$, and variances, $\mathrm{var}[\delta_k] = Q_k$ and $\mathrm{var}[\varepsilon_k] = R_k$. Then the UPF is obtained through the following steps of the pseudo-codes [5].

1. Initialization ($k = 0$): for $i = 1 : N$, draw the states (particles) $x_0^{(i)}$ from the prior $p(x_0)$, and set $\hat{x}_0^{(i)} = E[x_0^{(i)}]$ and $P_0^{(i)} = E[(x_0^{(i)} - \hat{x}_0^{(i)})(x_0^{(i)} - \hat{x}_0^{(i)})^{\mathrm{T}}]$.

2. For $k = 1, 2, \ldots$, carry out the following steps:

a. For $i = 1 : N$, update the particles using the UKF algorithm.

b. Sampling: for $i = 1 : N$, carry out importance sampling step. In this paper, sequential importance sampling (SIS) algorithm is included that is a Monte Carlo (MC) method that forms the basis for most sequential MC filters developed over the past decades [4]. In this paper, our goal is to perform filtering on the given models, i.e. to compute a sequential estimate of the posterior distribution at time step k without modifying the previously simulated states $x_{0:k-1}$ allowing proposal distributions of the form

$$q(x_{0:k}|z_{1:k}) = q(x_{0:k-1}|z_{1:k-1})q(x_k|x_{0:k-1}, z_{1:k}). \tag{33}$$

Assuming that the states follow a Markov process and that the observations are conditionally independent given the states yields

$$p(x_{0:k}) = p(x_0)\prod_{m=1}^{k} p(x_m|x_{m-1}) \tag{34}$$

$$p(z_{1:k}|x_{0:k}) = \prod_{m=1}^{k} p(z_m|x_m). \tag{35}$$

Sample:

$$\hat{x}_k^{(i)} \sim q(x_k^{(i)}|x_{0:k-1}^{(i)}, z_{1:k}) = N(x_k^{(i)}, P_k^{(i)}). \tag{36}$$

c. Set $x_{0:k}^{(i)} \triangleq (x_{0:k-1}^{(i)}, x_k^{(i)})$ and $P_{0:k}^{(i)} \triangleq (P_{0:k-1}^{(i)}, P_k^{(i)})$.
d. Importance weights: for $i = 1 : N$, evaluate the importance weights up to a normalizing constant i.e.,

$$w_k^{(i)} = w_{k-1}^{(i)} \frac{p(z_k|x_k^{(i)})p(x_k^{(i)}|x_{k-1}^{(i)})}{q(x_k|x_{0:k-1}, z_{1:k})}. \tag{37}$$

e. $i = 1 : N$, normalize the importance weights as

$$\tilde{w}_k^{(i)} = w_k^{(i)} \left[\sum_{m=1}^{N} w_k^{(m)}\right]^{-1}. \tag{38}$$

3. Re-sampling: fatefully, in SIS, the variance of the importance weights increases stochastically over time. The importance weights are proportional to the importance ratio, which variance increases over time [20]. In practice, what happens is that after a few time steps one of the normalized importance weights is close to 1 while the rest are close to 0. In other words, many the samples become useless and are neglected. To avoid this phenomenon, called degeneracy, the particles need to be re-sampled (selection step) to eliminate particles with low importance weights and multiply particles with high importance weights. Multiply/suppress samples $(\hat{x}_{0:k}^{(i)}, P_{0:k}^{(i)})$ with high/low importance weights $\tilde{w}_k^{(i)}$, respectively, to obtain N random samples $(\tilde{x}_{0:k}^{(i)}, \tilde{P}_{0:k}^{(i)})$.

4. Output: in Monte Carlo simulation, a set of weighted particles (samples), drawn from the posterior distribution, is used to map integrals to discrete sums. More precisely, the posterior can be approximated by the following empirical estimate

$$p(x_{0:k}|z_{1:k}) \approx \hat{p}(x_{0:k}|z_{1:k}) = \frac{1}{N}\sum_{i=1}^{N} \delta_{(x_{0:k}^{(i)})}(dx_{0:k}) \tag{39}$$

where the random samples $\{x_{0:k}^{(i)}; i = 1 : N\}$ are drawn form the posterior distributions and $\delta(d\cdot)$ denoted the Dirac delta function.

4. Simulation and results

Perhaps the earliest important application of the techniques of space navigation is the guidance of a ballistic missile. Guidance of a missile is accomplished by the most promising inertial systems. Inertial systems have the advantage of fast in-flight response and because they give good data on the short term changes in position and velocity, there is no need for long smoothing times with an inertial system [1]. An inertial navigation system possesses several favorable characteristics which make it desirable for use in a weapon system. It has all-weather capability and immune to electronic countermeasures directed against it. Its function is to determine the instantaneous position of the weapon system with respect to some reference point, and to generate signals that will make the weapon fly some desired trajectory to the target.

Like inertial systems, ANS is autonomous, requiring no outside facilities, except of course for the stars which are always there. Cloud cover is an obvious limitation for star sensors, and this relegates their usefulness to high altitude flight. Because it is a psi-angle measuring device, it basically updates the gyros and not the accelerometers. This means that acceleration errors can grow without bound [22].

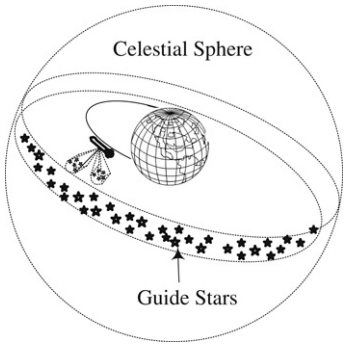

Fig. 5. The concept of ANS.

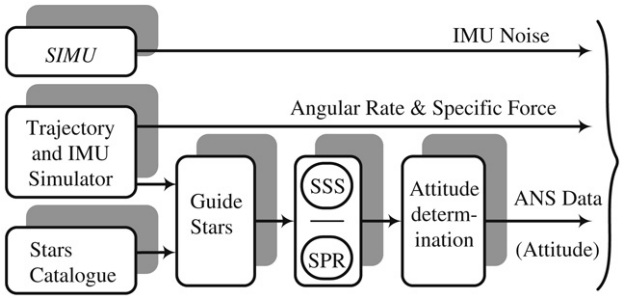

Fig. 6. Arrangement for simulation data.

The launch vehicle and missile trajectories are extremely sensitive to changes in characteristic attributes such as stage burnout time, altitude, velocity and orientation. A very small improvement in boost trajectory accuracy results in big gains in targeting accuracy. It should be clear that very small errors have very big consequences [23]. Consequently, small position and velocity errors at the cut-off point caused by gyro drift can be compensated by the proposed integrated navigation system. The concept of ANS is depicted in Fig. 5.

All the simulations have been carried out using Matlab. Here, SINS computations are carried out at 80 Hz, ANS aiding is provided at 1 Hz. Ballistic missile is a vehicle chosen for simulation of the presented integrated system. Simulations are carried out for the powered flight phase of the ballistic missile. ANS augmentation comes into effective 40 s after lift off of the missile when it attains altitude above 22 km from onwards stars are observable unobstructed [24].

4.1. Simulation data

To validate and corroborate the designed multisensor navigation data synthesis (MNDS) technique, simulation data is generated through a half physical simulation setup established in the laboratory [21]. The conceptual arrangement of this setup is depicted in Fig. 6. Simulation data consists of specific force, angular rate, ANS estimated attitude, and IMU noise.

In this setup, the missile trajectory and an IMU simulator are used to simulate flight path and the IMU outputs. The IMU outputs comprise angular rate and specific force. The ANS augmentation comes into effect about 40 s after lift off of the missile when it attains more than 22 km altitude, because at that altitude, stars are observable and unobstructed [24]. At this position, guide stars are extracted from the star catalogue stored in the computer. These guide stars are simulated using a physical star sensor simulator (SSS). The star's light is simulated on a liquid crystal display (LCD) and detected by the CCD electro-optical star sensor. Star pattern recognition (SPR) is carried out to identify the stars in the reference star catalogue. Once stars have been identified using a stars' identification technique, the attitude is estimated through a attitude determination procedure. An IMU placed statically on a stable base provides us with the noise due to imperfections in the gyroscopes and accelerometers employed [21].

4.2. Data averaging

Some enhancement in accuracy may be obtained when several measurements and their time intervals are averaged. An interesting special case arises when a sequence of positions have been measured at uniform time intervals following a reference time t. The sequence is given as [1].

$$r(t), r(t+\tau), r(t+2\tau), r(t+3\tau), \ldots, r(t+n\tau) \tag{40}$$

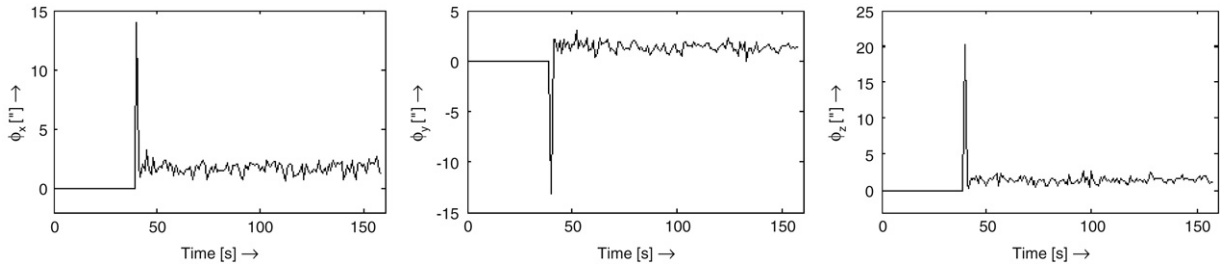

Fig. 7. Axes misalignment angles.

and the average velocity over the interval $n\tau$ may be calculated as

$$v = \frac{1}{n}\left[\frac{r(t+\tau)-r(t)}{\tau} + \frac{r(t+2\tau)-r(t+\tau)}{\tau} + \cdots + \frac{r(t+nt)-r[t+(n-1)\tau]}{\tau}\right] \tag{41}$$

$$v = \frac{1}{n\tau}\sum_{i=1}^{n}(r_i - r_{i-1}). \tag{42}$$

It is characteristic of this method of averaging that the effect of random errors in position measurement will be diminished in proportion to $\sqrt{n}$ when the velocity is calculated in this manner.

4.3. Figure-of-merit

A measure of the quality of SINS is some weighted combination of its attitude, position and velocity indication capabilities, depending upon the mission involved. The gyros measure the vector of inertial rotation and the system uses it to calculate attitude in the form of a coordinate transformation matrix. Inevitably, accelerometer and gyro errors occur in the measured vectors. As a result of gyro measurement error, an error in the transformation matrix occurs. Here, figure-of-merit (*fom*) is considered as a measure of gyro performance [14].

$$fom = \frac{1}{2}trace[(\delta C_b^{il})^{\mathrm{T}}\delta C_b^{il}]. \tag{43}$$

To demonstrate the significance of *'fom'*, the SINS computed direction cosine matrix will be perturbed as Eq. (12). The perturbed attitude matrix contains an error that represents an effective rotation of the indicated navigation axes relative to the true coordinates. Therefore, *'fom'* is evaluated in accordance with Eq. (43) using Eq. (13). In this manner, *'fom'* is related to the potential navigation errors caused by axes misalignment errors. Minimizing *'fom'* thus becomes a rational basis for optimum reduction in attitude errors.

4.4. Data synthesis filter initialization

For a medium accuracy SINS, the designed values of matrices for the process noise covariance Q and measurement noise covariance R are as follows:

$$Q = \mathrm{diag}([Q_{g_i}, Q_{a_i}]), \quad i = x, y, z$$

where $Q_{g_i} = (0.01^\circ/\mathrm{h})^2$ for gyros; and $Q_{a_i} = (50\ \mu\mathrm{g})^2$ for accelerometers

$$R = \mathrm{diag}([(20'')^2, (20'')^2, (20'')^2]).$$

Initial error covariance is defined as

$$P_0 = \mathrm{diag}([P_{\phi_i}, P_{v_i}, P_{r_i}, P_{\varepsilon_i}, P_{\nabla_i}]), \quad i = x, y, z$$

where $P_{\phi_i} = (10^{-4})^2$; $P_{v_i} = (0.1)^2$; $P_{r_i} = (10)^2$; $P_{\varepsilon_i} = (0.02^\circ/\mathrm{h})^2$; and $P_{\nabla_i} = (100\ \mu\mathrm{g})^2$.

4.5. Results

Simulations are carried out for the powered flight phase of the ballistic missile when it attains altitude well above the earth's atmospheric region. Fig. 7 shows the UPF estimated SINS misalignment angles. In Fig. 8, the UPF estimated gyros drifts are shown. The aforementioned results are plotted from 40 s after the lift-off to the cut-off time. Figure-of-merit as given in Section 4.3 is plotted in Fig. 9. Powered-flight trajectory of the ballistic missile is depicted in Fig. 10.

It is observed that a gyro induced error in velocity equal to 0.003% of cut-off velocity will cause significant errors in free-flight height, velocity, velocity angle, and difference between true anomaly and true anomaly at cut-off point. These errors are shown in Figs. 11–14. All these errors will end the vehicle's flight with a significant dispersion of the impact-point.

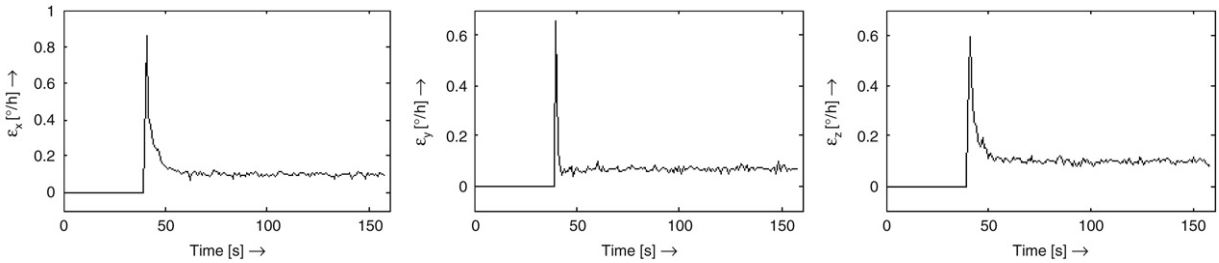

Fig. 8. Gyros drifts.

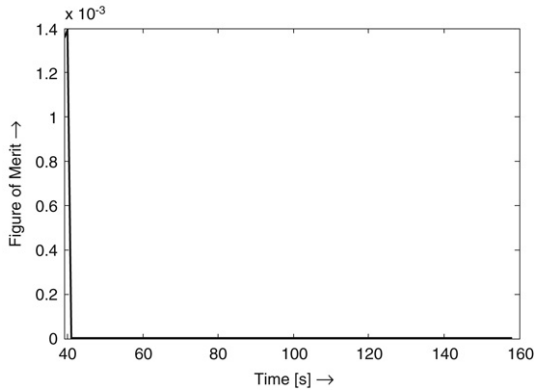

Fig. 9. Figure-of-merit.

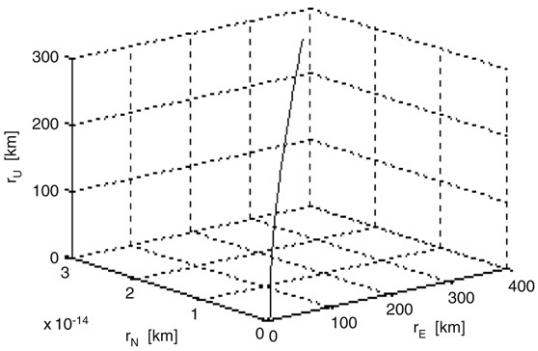

Fig. 10. Powered-flight trajectory.

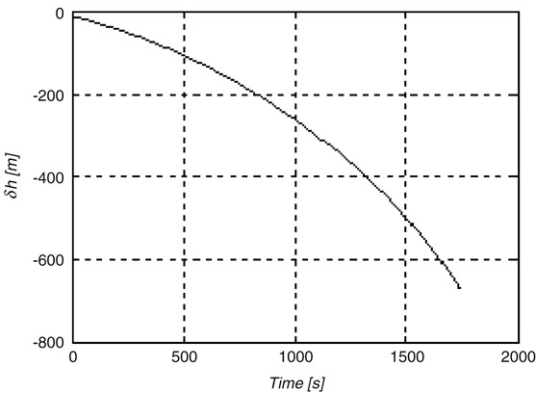

Fig. 11. Free-flight height error.

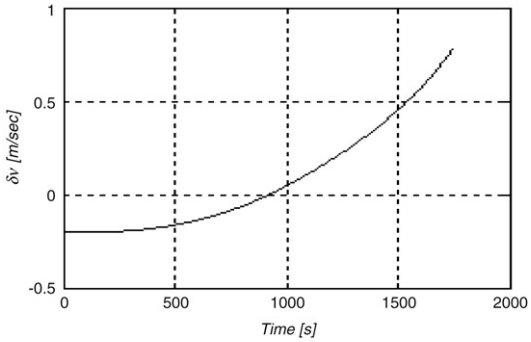

Fig. 12. Free-flight velocity error.

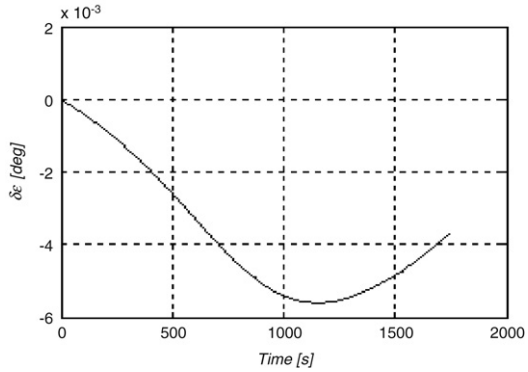

Fig. 13. Free-flight velocity angle error.

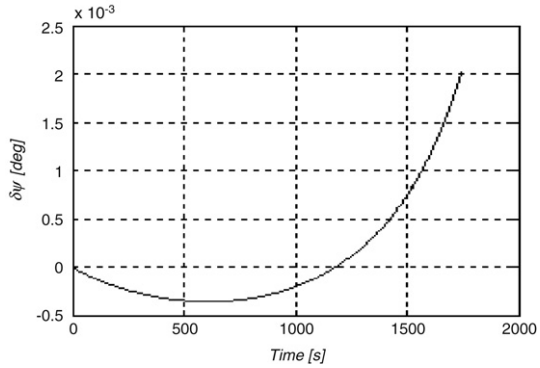

Fig. 14. Free-flight true anomaly error.

5. Conclusions

Accurate navigation systems often consist of several separate navigation systems which are integrated together to provide a more accurate and reliable navigation solution. The unscented particle filter is used to approximate the state a posteriori density in nonlinear and non-Gaussian filtering for integrated navigation with arbitrary accuracy. Because the particle filter is fairly easy to implement and tune, it has potential to become a popular tool in integrated navigation applications. Its main drawback is that it is quite computer intensive. For a given filtering accuracy, the computational complexity increases quickly with the state dimension. However, computational power has been tremendously increased during the past decades; the computational effort constraint in using the UPF has been reduced.

As observed, a gyro induced error in velocity at cut-off point will cause errors in free-flight height, velocity, velocity angle, and difference between the true anomaly and true anomaly at the cut-off point. All these errors will end the vehicle's flight with a significant dispersion of the impact-point. The ANS, as an autonomous augmentation suite for SINS, is used since their integrated performance outweighs the shortcomings of the individual systems. This integration results in estimation

of attitude errors and thus compensation of gyros drift, and velocity and position errors caused by the gyros drift. Therefore, SINS/ANS solution can be used for extended periods without degradation.

References

[1] E.V.B. Stearns, Navigation and Guidance in Space, Prentice-Hall, Inc., Englewood Cliffs, NJ, 1963.
[2] M. Fernandez, G.R. Macomber, Inertial Guidance Engineering, Prentice-Hall, Inc, Englewood Cliffs, NJ, 1962.
[3] W.J. Jun, G.I. Jun, A tightly coupled GPS/INS integration based on the unscented particle filter, in: Proceedings of the 2004 International Symposium on GNSS/GPS Sydney, Australia 6–8 December 2004.
[4] B. Ristic, S. Arulampalam, N. Gordon, Beyond the Kalman Filter: Particle Filters for Tracking Applications, Artech House, 2004.
[5] R. van der Merwe, A. Doucet, N. Freitas, E. Wan, The unscented particle filter, Technical Report CUED/F-INFENG/TR 380, Cambridge University Engineering Department, August 2000.
[6] C. Arbinger, W. Enderle, Spacecraft attitude determination using a combination of GPS attitude sensor and star sensor measurements, ION GPS 2000, 19–22 September 2000, Salt Lake City, UT, pp. 2634–2642.
[7] K.R. Britting, Inertial Navigation Systems Analysis, Wiley-Interscience, New York, 1971.
[8] Y.L. Xiao, Foundation of flight dynamics-modeling of aerospace vehicle motion, Beijing University of Aeronautics and Astronautics Press, 2003 (in Chinese).
[9] T.L. Lindsay, An inertially guided missile with mid-course re-alignment, M.Sc. Thesis, MIT, 1961.
[10] H.K. Lee, J.G. Lee, C.G. Park, Y.K. Rho, Modeling quaternion errors in SDINS: Computer frame approach, IEEE Transactions on AES 34 (1) (1998) 289–299.
[11] F. Bernard, Analysis strapdown navigation using quaternion, IEEE Transactions on Aerospace and Electronics Systems 14 (5) (1978) 764–768.
[12] M.J. Yu, J.G. Lee, H.W. Park, Comparison of SDINS in-flight alignment using equivalent error models, IEEE Transactions on Aerospace and Electronics Systems 35 (3) (1999) 1046–1054.
[13] R.A. Nash, S.A. Levine, K.J. Roy, Error analysis of space-stable inertial navigation systems, IEEE Transactions on Aerospace and Electronic Systems 7 (4) (1971) 617–629.
[14] A. Gelb, A.A. Sutherland, Design approach for reducing gyro-induced errors in strapdown inertial systems, AIAA 68–830.
[15] R.M. Rogers, Applied Mathematics in Integrated Navigation Systems, second ed., American Institute of Aeronautics and Astronautics, Inc., Reston, Virginia, USA, 2003.
[16] J. Ali, J.C. Fang, In-flight alignment of inertial navigation system by celestial observation technique, in: Proc. International Symposium on Inertial Navigation Technology and Intelligent Traffic, Nanjing, China, October 2004.
[17] J.E. Handschin, D.Q. Mayne, Monte Carlo techniques to estimate the conditional expectation in multi-stage non-linear filtering, International Journal of Control 9 (5) (1969) 547–559.
[18] J.E. Handschin, Monte Carlo techniques for prediction and filtering of nonlinear stochastic processes, Automatica 6 (1970) 555–563.
[19] T. Huillet, G. Salut, Interpretation des equations du filtrage non-lineaire, In Siances du GDR Automatique du CNRS (Pde non-liniaire), Paris, Nov. 8, 1989.
[20] A. Doucet, N.J. Gordon, V. Krishnamurthy, Particle filters for state estimation of jump Markov linear systems, Technical Report CUED/FINFENG/TR 359, Department of Engineering, Cambridge University, 1999.
[21] W. Quan, J.C. Fang, Hardware-in-the-loop simulation of celestial navigation system, in: Proc. 12th Saint Petersburg International Conference on Integrated Navigation Systems, Russia, 2005.
[22] C.F. Lin, Modern Navigation, Guidance, and Control Processing, Prentice hall, Englewood Cliffs, New Jersey, 1991.
[23] L.E. McKinney, Testimony to the committee on science. http://www.fas.org/nuke/intro/missile/basics.htm.
[24] S. Levine, AGARDograph on advanced astroinertial navigation systems, AGARD-AG-331, Aerospace Navigation Systems, 1995, pp. 187–199.